DESIGN AND EXPERIMENT OF ARRAY-BASED FINGERPLATE DIFFERENTIAL FLOW SENSOR FOR RICE GRAIN MONITORING
/
阵列式指板差分水稻籽粒流量传感器的设计与试验

Qibin LI[1)], Yang YU[1)], Gang GUO[2)], Jinpeng HU[1)], Peng LIU[1)], Xiaoyu CHAI[1)], Yingfeng WANG[1)], Lizhang XU[1*)]
[1)] College of Agricultural Engineering, Jiangsu University, Zhenjiang 212013, China
[2)] Zoomlion Heavy Industry Science & Technology Co., Ltd Changsha 410013, China
Correspondence email: justxlz@ujs.edu.cn
DOI: https://doi.org/10.35633/inmateh-74-31

Keywords: *Grain Flow Sensor; Auger elevators; Array Structure; Dual-Plate Differential; Random Forest*

ABSTRACT

Most existing grain flow sensors are designed for paddle-type elevators, with limited focus on applications in auger elevators. This paper addresses the yield monitoring needs during rice harvesting operations, specifically targeting auger-based outlets through experimental research. An array-type differential grain flow sensor was developed and an indoor test bench was constructed to evaluate its performance. The study compares the effectiveness of time-domain and frequency-domain differential processing, alongside various filtering methods, for pre-processing the sensor's raw signals. Additionally, a grain flow regression model was built using the Random Forest algorithm. Experimental results demonstrated that the monitoring errors during field tests ranged from -6.42% to 8.23%, indicating that the sensor met the requirements for rice yield monitoring. This sensor provides valuable data for feed rate detection, speed regulation, and adjustments to the threshing and cleaning systems in combine harvesters, offering significant practical implications for the promotion and development of precision agriculture.

摘要

现有的籽粒流量传感器大多面向于刮板式升运器，鲜有针对搅龙式升运器工作场景的籽粒流量传感器。本文面向搅龙式出粮口，针对水稻收获作业的产量监测需求进行试验研究，开发了阵列式指板差分结构的籽粒流量传感器，研制了籽粒流量传感器室内试验台，对比了时域、频域差分处理以及不同滤波方法对所采集的传感器原始信号的预处理效果，并基于随机森林算法构建了籽粒流量回归模型。试验结果表明田间试验监测误差为-6.42%~8.23%，能够满足水稻收获的产量监测需求，可以为联合收获机喂入量检测、前进速度调控或者脱粒清选装置的作业参数调节提供数据参考，对精准农业的推广和发展也具有重要的实际意义。

INTRODUCTION

The mapping of grain yield during harvesting operations is a crucial component of precision agriculture, and an accurate and reliable grain flow monitoring sensor is fundamental for generating yield distribution maps *(Vinod Chandra et al., 2024; Kasera et al., 2024)*. With advancements in sensor and GPS technologies, yield monitoring systems have been widely adopted in Europe and the United States *(Yin et al., 2024)*. In these regions, large wheeled harvesters are commonly used, which often incorporate scraper elevators that allow for high grain flow rates and concentrated impact areas, making signal acquisition relatively straightforward *(Cheng et al., 2023)*. However, in the Huang-Huai-Hai region of China, a rotation system of rice and oilseed or rice and wheat is typically implemented. In this context, compact and highly adaptable tracked harvesters have become the mainstream model for rice harvesting in southern paddy fields *(He et al., 2023)*. These machines generally employ auger-type elevators for grain transport, as illustrated in Fig. 1.

According to the measurement principle, yield detection methods can be categorized into types such as mass measurement and volume measurement. Among these, the impulse-based grain flow sensor, which falls under mass measurement, has become one of the most widely used measurement methods due to its simple structure, ease of installation, and low cost *(Bantchina et al., 2024)*. In the research on impulse-based grain flow sensors, *Hu et al (2009)* designed a dual-plate differential impulse grain flow sensor to address vibration interference, effectively mitigating the impact of vehicle vibrations on measurement accuracy.

Qibin Li (M.Eng. student), Yang Yu (Research Associate), Gang Gu (Engineer), Jinpeng Hu (Doctor), Peng Liu (Doctor), Xiaoyu Chai (Research Associate), Yingfeng Wang (M.Eng. student), Lizhang Xu (Professor)

Liu et al (2018) developed a dual-plate differential impulse grain flow sensor with a curved impact plate based on the scattering patterns of grain from scraper elevators. They conducted a spatiotemporal analysis of yield distribution data collected over two consecutive years in the same field. *Li et al (2015)* analyzed the impact patterns of grains, determined the optimal sampling frequency based on the sampling theorem, and compared two different signal processing methods: double-threshold filtering and arithmetic mean. *Wei et al (2014)* addressed the issue of vibration noise interference in impulse grain flow sensors by employing signal dual-plate differential techniques and wavelet transformation for filtering the raw signals. *Shoji et al (2009)* established a nonlinear grain flow model suitable for local combine harvesters in Japan, which, after validation through yield tests, demonstrated a relative root mean square error of 4.4% when the elevator speed was stable.

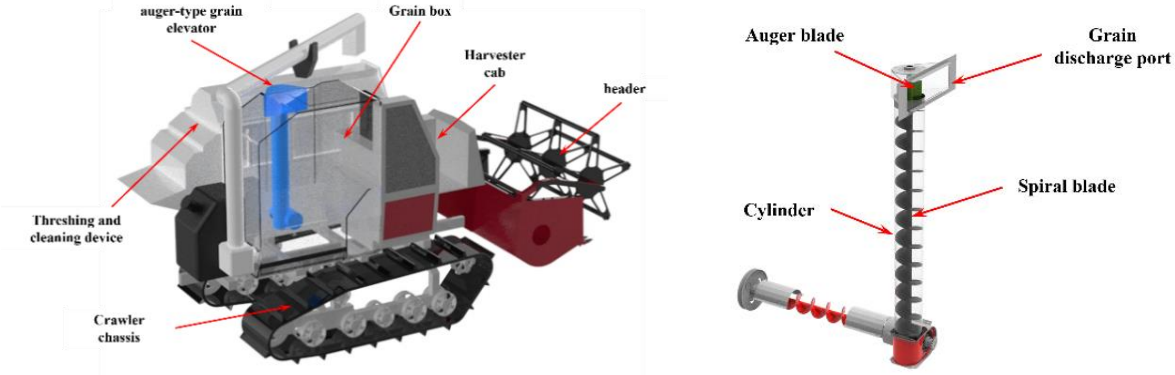

(a) Crawler combine harvester (b) Auger conveyor

Fig.1 - Grain conveying system of the crawler combine harvester

In summary, existing impulse flow sensors rarely address applications in auger elevators. Therefore, this study focuses on the auger elevator of tracked combine harvesters, designing an array-type paddle impact grain flow sensor. The signal processing method was optimized to enhance vibration interference resistance through frequency-domain differential processing and filtering. A grain flow regression model was constructed based on the Random Forest algorithm. Finally, field tests were conducted during rice harvesting using the self-developed grain flow sensor, achieving online monitoring of yield information throughout the harvesting process.

MATERIALS AND METHODS

Design of the Grain Flow Sensor Structure

Compared to scraper elevators, auger elevators convey a smaller grain flow and exhibit a less concentrated scattering of grains at the discharge outlet. To identify the optimal installation position for the sensor, the scattering distribution characteristics of grains at the discharge outlet was analyzed and EDM simulations of the grain transport process in auger elevators were conducted. The simplified auger model was imported into EDEM software (2021, Altair Engineering Inc., Troy, MI, USA), with the auger speed set at 860 rpm. A particle factory was established at the base of the auger, and data was saved at a time step of 0.01 seconds over a total simulation time of 5 seconds. The mechanical property parameters of the rice grains and the contact coefficients of the working components were set based on the literature *(Zhao et al., 2023; Ma et al., 2023; Xing et al., 2024)*. The scattering distribution of rice grains under different flow rates is illustrated in Fig. 2. The simulation results indicate that the rice grains scatter in a fan-shaped distribution, flowing along the side walls of the auger and falling into the grain tank, while the middle area experiences wave-like scattering of grains influenced by the auger blades. It is clear that monitoring all grain impact signals at the outlet would require a sensor monitoring plate with a large surface area, which could interfere with the normal flow of grains into the tank and even block the auger outlet.

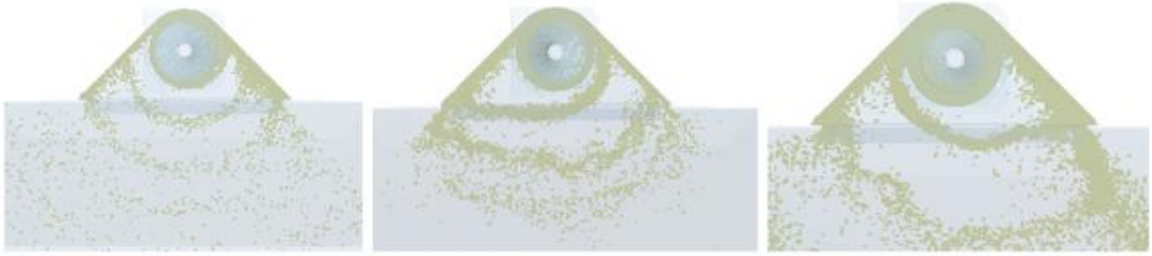

(a) Grain flow rate at 0.5 kg/s (b) Grain flow rate at 1.5 kg/s (c) Grain flow rate at 2.5 kg/s

Fig. 2 - Rice Grain Discharge Characteristics at Different Flow Rates

To address this challenge, a multi-point monitoring method using dual-plate differential sensors, leading to the development of a custom grain flow monitoring sensor, as illustrated in Fig. 3, is proposed. The sensor is organized into three monitoring units: left, center, and right. Each unit consists of an impact paddle sensor and a reference paddle sensor. These paddle sensors are designed with point pressure sensors and paddles, secured by a gantry installation bracket and universal vibration-damping steel wires. All paddles are constructed from stainless steel. The impact paddle sensor captures the force from the grain flow, while the reference paddle sensor monitors vibrations and zero-point drift in that location. The front and rear paddles are parallel and do not make contact, with their sides bent at a 90° angle to enhance their strength. The universal vibration-damping steel wires help mitigate interference from vibrations during harvesting operations.

To ensure that the monitoring units on both sides receive normal impacts from the grain flow, the left and right sensors are installed perpendicular to the auger discharge outlet, while the center sensor is positioned parallel to it. The monitoring surfaces of the left and right units form an angle of 35.5° with the surface of the center unit, creating a symmetrical arrangement. Each paddle has an area of 135 × 40 mm, and the pressure sensors are single-point types (AT8501, AUTODA, China) with a maximum capacity of 300 grams, based on the design parameters derived from our earlier simulation analysis

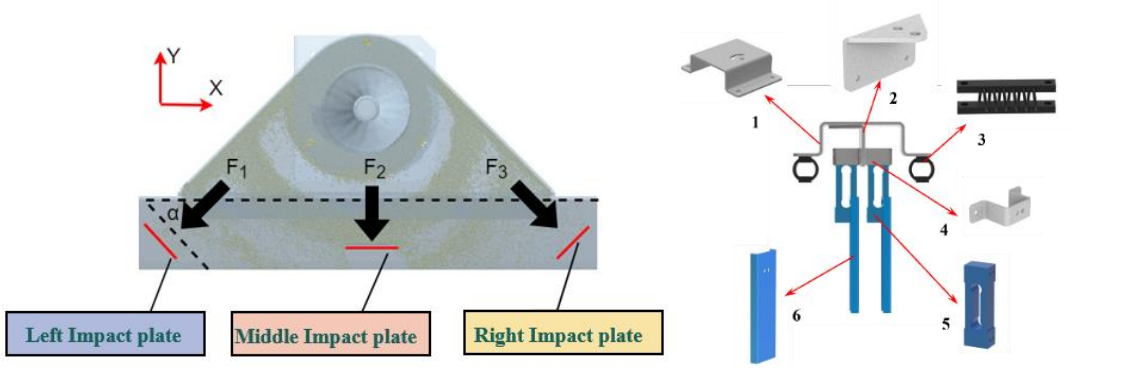

(a) Sensor Installation Position and Force Direction (b) Components of the Sensor Monitoring Unit

Fig. 3 - Differential Grain Flow Sensor with Array Structure

1 - Gantry mounting bracket. 2 - Mounting plate. 3 - Universal damping steel wire. 4 - Small gantry bracket. 5 - Pressure sensor. 6. Plate.

Sensor signal conditioning circuit design

The hardware circuit of the array-type paddle differential flow sensor primarily consists of a power supply circuit, measurement circuit, differential amplification circuit, and bandpass filtering circuit, as illustrated in Fig.4.

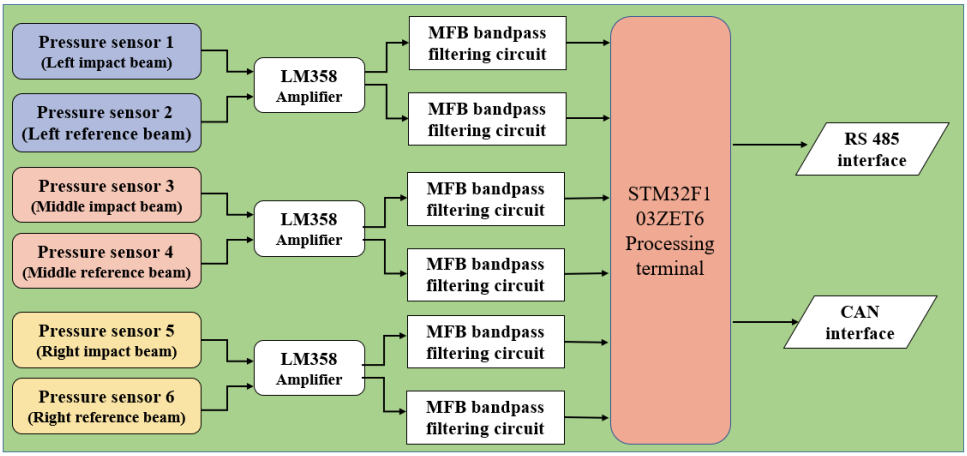

Fig. 4 - Hardware Circuit Diagram

The AT8501 pressure sensor generates only 10 mV of voltage under a 5 V excitation voltage with a 300 g load, necessitating the use of an LM358 amplification chip to enhance the weak signal. Given that the amplified strain signals require bandpass filtering, the choice of cut-off frequencies significantly affects the measurement accuracy of the sensor. Therefore, an adjustable center frequency second-order multiple feedback bandpass filter is utilized to meet the dynamic flow monitoring requirements. To facilitate the recording and analysis of experimental data, the sensor can directly output real-time flow signals via RS-485 or CAN communication after processing the signals within the microcontroller.

Development of the Grain Flow Indoor Test Bench

To further shorten the development cycle, this study developed an indoor grain flow test bench to simulate the grain conveying conditions of a tracked combine harvester in the field. The dimensions of the auger blades and the inner diameter of the auger cylinder match those of the 4LZ-6.0 combine harvester and are capable of achieving the machine's rated auger speed. The test bench enables calibration of the relationship between grain flow rate and sensor electrical signals and allows for the acquisition of background vibration noise to explore optimal noise reduction methods.

The physical setup of the grain flow test bench, shown in Fig. 5, consists primarily of the following components: an array-type differential flow sensor, a material receiving frame, a vertical auger, a measuring device, a grain hopper, a three-phase AC asynchronous motor, a frequency converter, and an opening adjustment flap. During the test, grains in the hopper are pushed by a horizontal auger to the bottom of the vertical auger, lifted to the auger outlet, and then discharged into a glass receiving frame. A funnel below the receiving frame, equipped with a load cell-based measuring device, records the cumulative change in grain mass, allowing for the calculation of key information such as the average flow rate. The grain flow rate is adjusted using a flap at the bottom of the hopper.

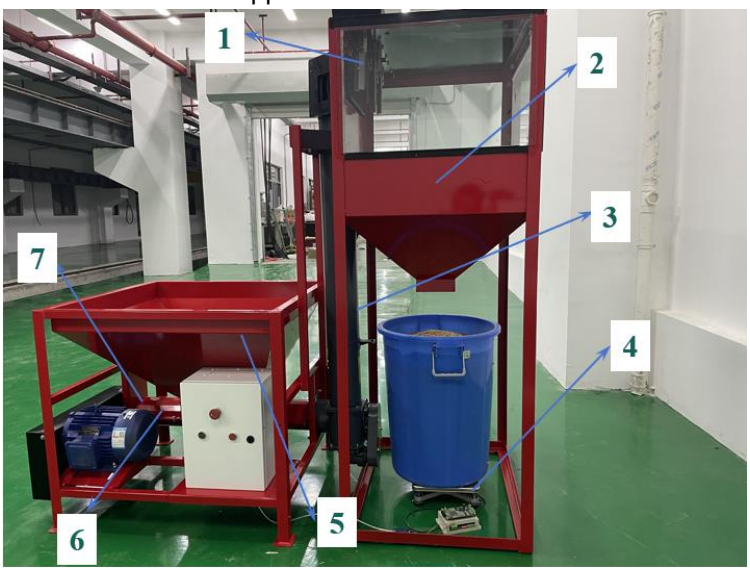

Fig. 5 - Test bench for the flow sensor experiment

1 - Flow sensor. 2 - Material receiving frame. 3 - Auger grain elevator. 4 - Measuring device. 5 - Grain hopper. 6 - Three-phase AC asynchronous motor and frequency converter. 7 - Opening adjustment baffle.

Sensor Signal Differentiation and Denoising

To ensure that the vibration and impact amplitudes of all sensors are on the same scale, static calibration of each sensor was conducted using standard weights. As shown in Fig. 6(a), standard weights were applied at random positions on the monitoring paddles to obtain the static force characteristic curves for each sensor, illustrated in Fig. 6(b). The output signals from the six parallel beam pressure sensors demonstrated excellent linearity within their measurement range, meeting the required specifications for use.

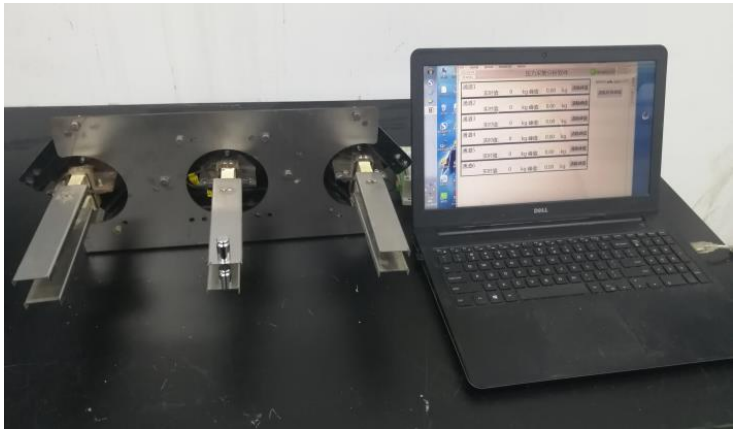

(a) Static calibration test

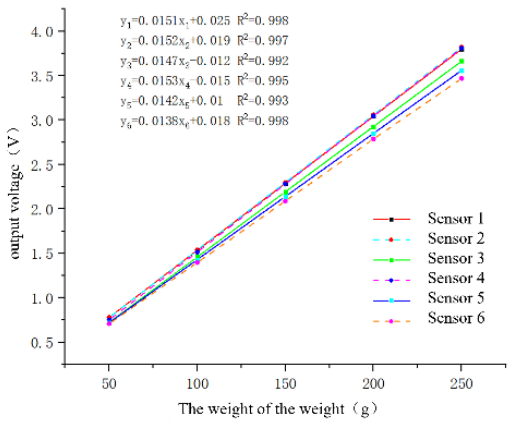

(b) Static force characteristics

Fig. 6 - Static calibration of the pressure sensors

Damping alone cannot completely eliminate the influence of vibrations; therefore, the raw vibration signals from the sensors mounted on the machine were collected and the vibration signals from each differential unit in both the time domain and frequency domain were processed to compare the denoising effects. The signals detected by the impact paddle sensor and the vibrations measured by the reference paddle sensor represent a pair of common-mode signals. To ensure the effectiveness of the signal differentiation, the original signal acquisition frequency for the pressure sensors was set to 500 Hz, in accordance with the Nyquist sampling theorem, during the collection of vibration signals under no-load conditions. The collected raw signals are depicted in Fig. 7, with time-domain and frequency-domain differential analyses performed on the original output signals from the three paddle groups, as shown in Figs. 8 and 9.

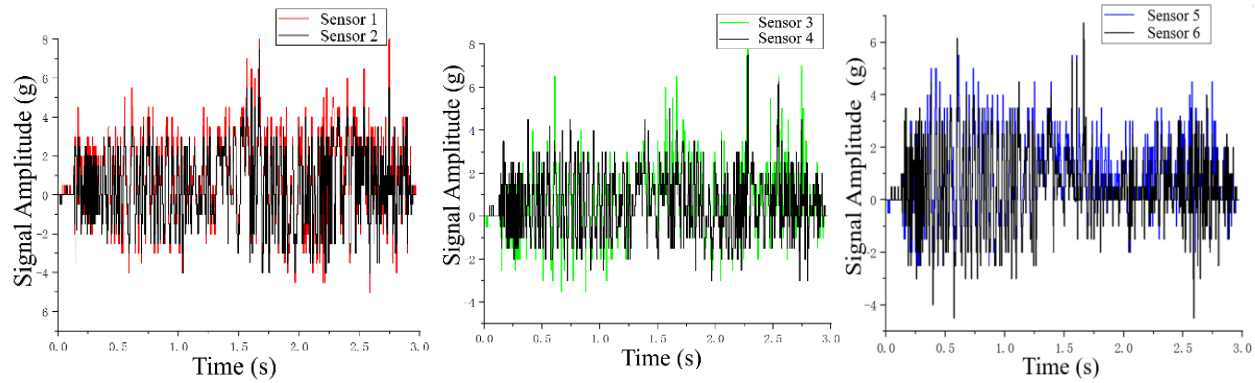

(a) Left monitoring unit (b) Middle monitoring unit (c) Right monitoring unit

Fig. 7 - The original vibration signal of each monitoring unit

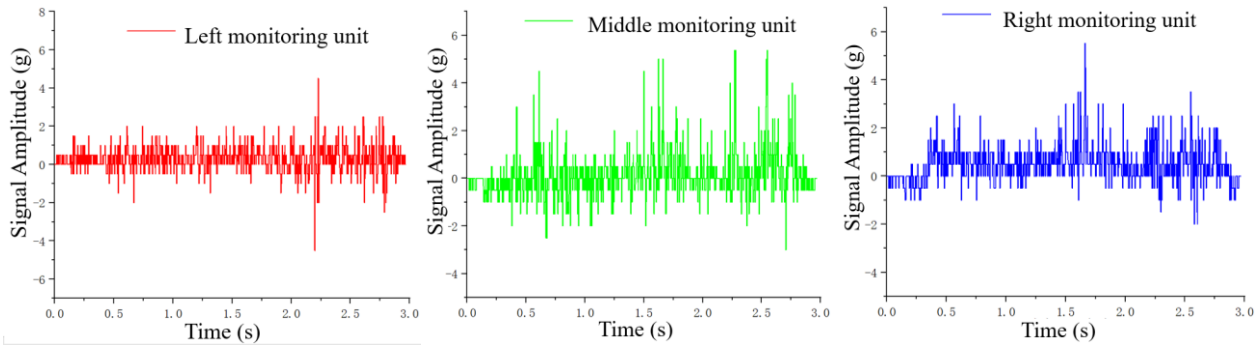

(a) Left monitoring unit (b) Middle monitoring unit (c) Right monitoring unit

Fig. 8 - Time domain difference signal of each monitoring unit

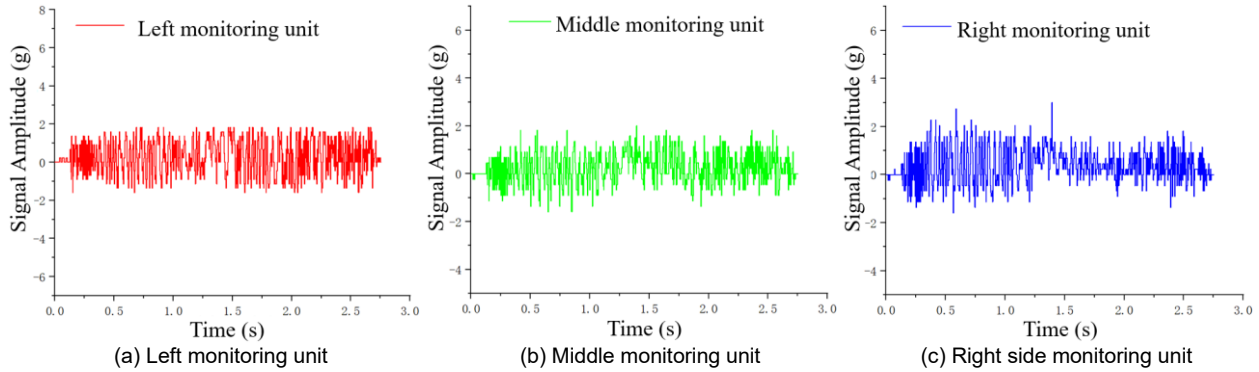

(a) Left monitoring unit (b) Middle monitoring unit (c) Right side monitoring unit

Fig. 9 - The frequency domain differential signal of each monitoring unit

As shown in Fig. 7, it is evident that the vibration amplitudes of each paddle in the raw signal under no-load conditions are similar, yet the signal concentration varies and exhibits significant oscillations. After performing time-domain differentiation, the amplitudes, means, and standard deviations of the signals from each monitoring unit decreased, resulting in improved signal concentration and demonstrating effective differentiation. However, the phase subtraction in the time domain does not completely eliminate sudden changes in acceleration, as some peaks still remain. In contrast, conducting signal differentiation in the frequency domain effectively reduces the frequency of peak occurrences, preventing peaks exceeding 6 g.

A further comparison of the mean and standard deviation between frequency-domain and time-domain differencing, as shown in Table 1, indicates that the mean and standard deviation of the signals from the left, middle, and right monitoring units all decreased. This suggests that frequency-domain differencing significantly improves the signal concentration during the impact phase, and the effect of background vibration noise reduction for each monitoring unit's sensor is relatively stable.

Table 1

Mean and variance of each sensor

Monitoring unit	Left monitoring unit		Middle monitoring unit		Right monitoring unit	
Sensor number	Time Domain	Frequency Domain	Time Domain	Frequency Domain	Time Domain	Frequency Domain
Signal average /g	0.29	0.26	0.25	0.15	0.48	0.38
Signal standard deviation /g	0.72	0.71	1.02	0.66	0.79	0.74

Sensor Signal Filtering and Noise Reduction

The grain flow consists of discrete particle flows, which, when combined with background noise generated by machine vibrations, results in signals obtained through frequency-domain differentiation that are not entirely stable. To further enhance monitoring accuracy, additional filtering of the signals is required. Therefore, this study employs various filtering algorithms for secondary filtering based on the frequency-domain differentiated signals, aiming to identify the optimal secondary filtering method.

The data acquisition process during the bench tests is as follows: the motor speed is controlled, and each trial involves pre-weighing 40 kg of rice grains to be fed into the hopper. The opening of the adjustment baffle is fixed to regulate the flow rate to approximately 1.5 kg/s, with three repetitions of each trial. This study evaluates nine different filtering methods for secondary filtering, with their effects illustrated in Fig. 10.

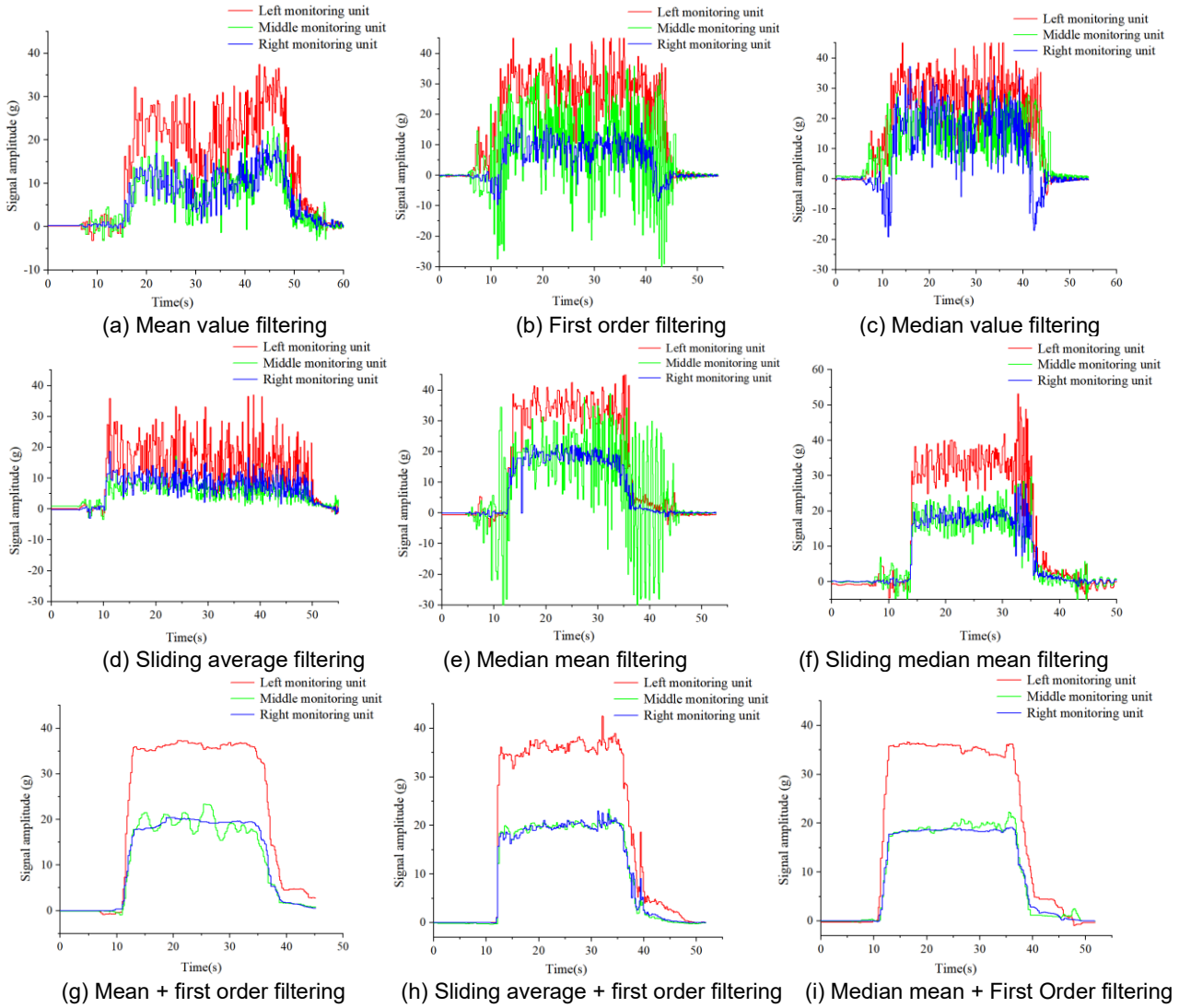

(a) Mean value filtering (b) First order filtering (c) Median value filtering

(d) Sliding average filtering (e) Median mean filtering (f) Sliding median mean filtering

(g) Mean + first order filtering (h) Sliding average + first order filtering (i) Median mean + First Order filtering

Fig. 10 - Effects of different secondary filtering methods

The initial assessment of the above data indicates that the performance of first-order filtering, average filtering combined with first-order filtering, sliding average filtering combined with first-order filtering, and median average filtering combined with first-order filtering is relatively satisfactory.

To further compare the filtering effects, the ratio of the sum of the monitoring values (Sum) from the secondary filtering to the mass of the input grains (m), referred to as the conversion coefficient (k) under flow conditions is evaluated. By comparing the standard deviation of the conversion coefficient (k), the effectiveness of the various filtering methods can be determined.

As shown in Table 2, the standard deviation of the ratio Sum/m is smallest for median average filtering combined with first-order filtering among the various filtering methods. The grain flow impacts the impact plates in a non-simultaneous and discrete manner over time, which, when combined with machine vibrations, leads to high-frequency fluctuations in the original signal. Median average filtering dynamically removes extreme values from the collected data, mitigating sampling deviations caused by occasional impact disturbances, and effectively reduces measurement errors of the flow sensor. The subsequent application of first-order filtering after median average filtering leverages its advantage in high-frequency data acquisition and provides good suppression of periodic vibration interference from the combine harvester's working components.

Table 2

Comparison of the different secondary filtering effects of three crops

Secondary filtering method	Standard deviation of *k*		
	Left group	Middle group	Right group
First order filtering	46.75	110.65	132.91
Mean + First order filtering	79.936	41.19	56.52
Sliding average filtering + First order filtering	68.35	148.87	62.74
Median mean filtering + First order filtering	58.63	41.25	52.76

In summary, the signal processing flow for the sensor is as shown in Fig. 11: the signals from each monitoring unit are differentiated in the frequency domain, transformed into three independent time-domain signals through inverse discrete Fourier transform, and then subjected to secondary filtering (median average filtering combined with first-order filtering) to achieve stable monitoring signals.

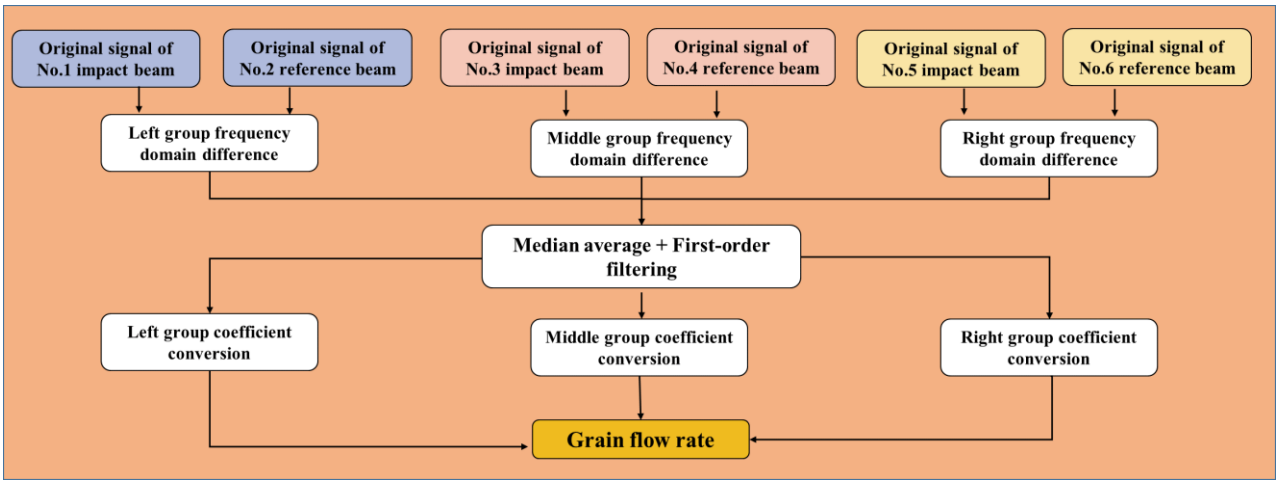

Fig. 11 - The signal processing flow of the flow sensor

RESULTS AND ANALYSIS

Establishment of the grain flow measurement model

To establish a mathematical metering model for grain flow, this study collected sensor signals from the grain flow test bench, capturing the output signals from three monitoring unit sensors along with the changes in accumulated mass of rice grains at various flow rates, as illustrated in Fig. 12.

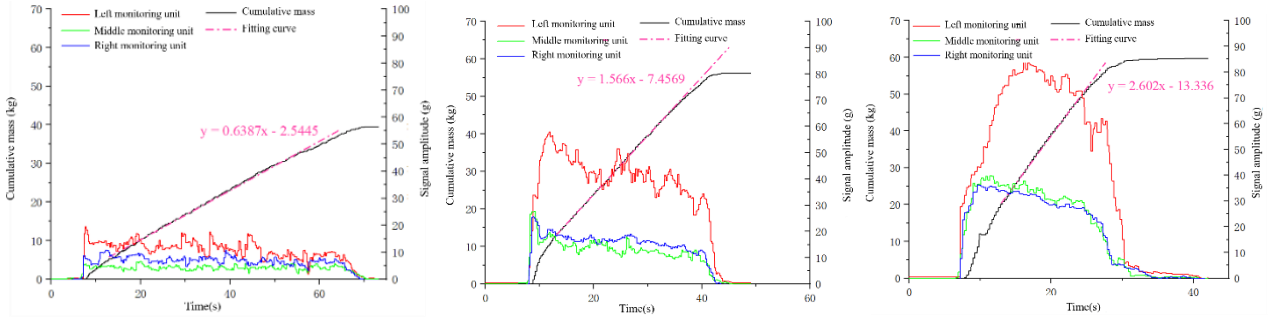

(a) 0.64 kg/s (rice) (b) 1.57 kg/s (rice) (c) 2.60 kg/s (rice)

Fig. 12 - Changes in the rice accumulative quality and signal amplitude of each monitoring unit under different flow rates

It can be observed that the signal amplitude of the monitoring units is correlated with the slope of the cumulative mass curve. The significant differences in signal amplitude among the left, middle, and right units are attributed to the orientation of the vertical grain auger. The auger blades are tilted leftward, with a counter clockwise rotation (viewed from above), causing the right fan blades to throw grains towards the left side, as shown in Fig. 13(a). As the flow rate increases, the fill level within the auger blades rises, resulting in more grains being dispersed towards the left and middle monitoring units, specifically in the ∠AOD region shown in Fig. 13(b). This indicates that the flow rate variations at the three monitoring positions are not synchronized, making it unreasonable to represent the overall grain flow rate based on a single monitoring location.

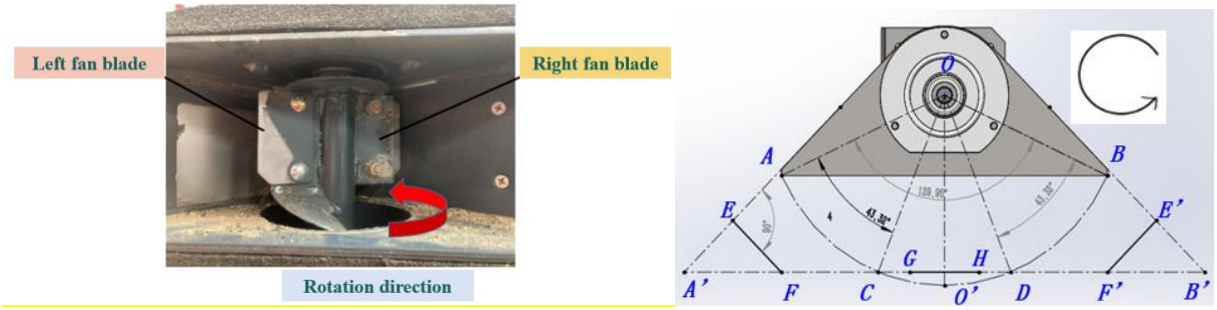

(a) Position distribution of the auger blades (b) Schematic diagram of the monitoring areas

Fig. 13 - Position distribution of the auger blades

For the designed array-type paddle differential flow sensor, the differing amplitudes of signals from the left, center, and right monitoring units indicate that the gain varies under the same flow conditions. This suggests that the three monitoring units correspond to three distinct fan-shaped regions where the distribution of grain dispersion is uneven. Traditional linear or multivariate nonlinear regression methods do not yield satisfactory results for flow regression modelling. In contrast, the Random Forest algorithm offers advantages such as parallel processing, low computational overhead, fewer parameters to adjust, and ease of implementation compared to other common machine learning methods *(Zhou et al., 2023; Ravishankar et al, 2023)*.

Therefore, this study employs the Random Forest algorithm to establish a regression model for grain flow.

It is important to note that due to the poor fluidity of the grains, the descent speed of the rice grains in the feed hopper decreases with pressure, resulting in an overall declining trend in the amplitudes of the three monitoring units under the same opening. Consequently, using the long-time interval change in cumulative mass Δm to represent the true flow is not reasonable. During the stable flow phase from t_1 to t_2, the sum of the signal amplitudes S from each monitoring unit over a unit time interval Δt is positively correlated with the average flow rate Q over that time interval. The model is constructed as follows:

$$y = f(x_1, x_2, x_3) \tag{1}$$

In the equation, y represents the grain flow rate per unit time Δt, and x_1, x_2 and x_3 are the values of $S/\Delta t$ for the left, middle, and right monitoring units, respectively. The model for the average grain flow rate Q within Δt t is given by:

$$\frac{\Delta m}{\Delta t} = f\left(\frac{S_1}{\Delta t}, \frac{S_2}{\Delta t}, \frac{S_3}{\Delta t}\right) \quad (2)$$

Due to the continuous variation in signals from the three monitoring units, the sum of the signal amplitudes S per unit time also changes accordingly. This implies that time displacement in the time domain will result in changes to the "rectangular" area S of each monitoring unit's signal, which, in turn, causes slight variations in Δm due to deviations in the cumulative mass data. By selecting different unit time steps Δt, a more diverse set of samples can be created, as shown in Fig. 14. Additionally, there is a small amount of zero drift at the beginning and end of the experiment, with the drift amount within 0.5 g. Data from this time period can be used to construct zero drift samples, which are represented as follows:

$$\frac{\Delta m}{\Delta t} = 0 = f\left(\frac{S_1}{\Delta t}, \frac{S_2}{\Delta t}, \frac{S_3}{\Delta t}\right) \quad (3)$$

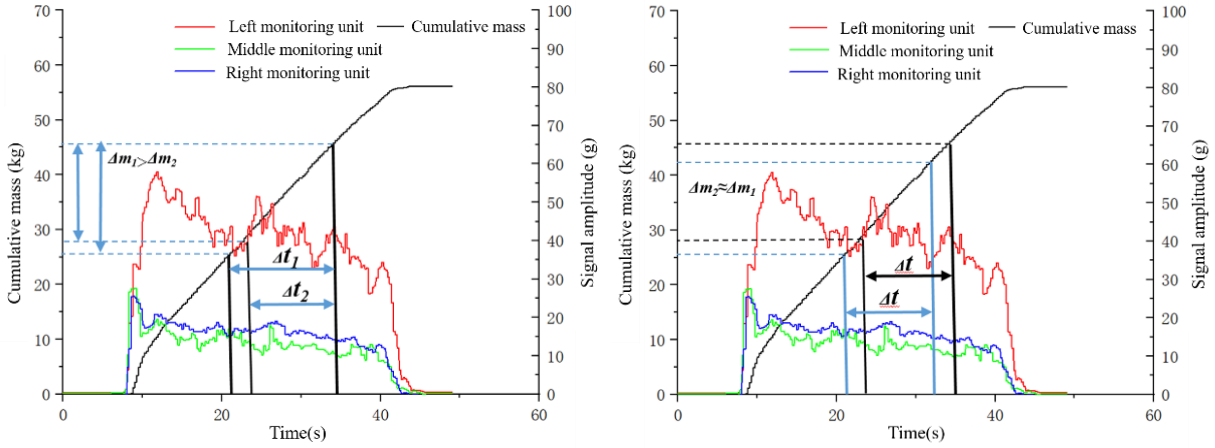

(a) Method for changing Δt (b) Method for maintaining a fixed Δt

Fig. 14 - Construction of the original dataset

In field harvesting operations, the complexity of zero-drift caused by machine start-stop, turns, and other conditions makes it more challenging to filter zero-drift data from linear models compared to bench tests. However, this issue can be easily addressed in a random forest regression model.

Therefore, the sample construction for the random forest regression model only needs to focus on the following time points: the point where the cumulative mass curve begins to change slope, indicating that grains have started to be discharged from the outlet but remain unstable. This point is denoted as t_R, any sensor signals before this point are considered as zero-drift data. The moment when the testing platform reaches its rated speed, at which point the grain discharge becomes relatively stable. This moment is noted as t_1.

The time when the screw conveyor begins to show a significant decrease in grain flow, with clear reductions in sensor data and the cumulative mass curve's slope gradually approaching zero. This moment is recorded as the end of stable flow, noted as t_2. After t_2, the slope of the cumulative mass curve remains at zero. The initial time when this occurs is denoted as t_S, continuing until the end of data collection at t_N. The period from t_S to t_N represents the zero-drift phase. The divisions of these time periods are illustrated in Fig.15.

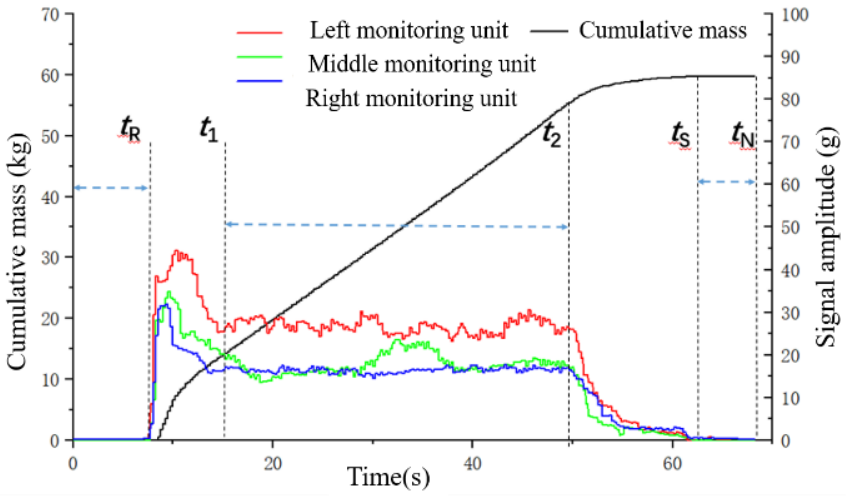

Fig. 15 - The division of the time periods of a single group of experimental data

After selecting specific time periods, an array $[x_1, x_2, x_3, y]$ is constructed using Formula 2, where y represents the grain flow within the time interval Δt, and x_1, x_2 and x_3 correspond to the values of $S/\Delta t$ from the left, middle, and right monitoring units, respectively.

Choosing a very small flow calculation period Δt can increase computational load and lead to sample bias, especially under high flow conditions. Conversely, a very large Δt may fail to capture flow variations adequately. To determine the optimal size of Δt, this study selected 0.4 s, 0.8 s, and 1.2 s as candidate parameters. After obtaining the samples, the rice regression model is established. 80% of the dataset is used for training, while 20% is used for testing. The depth of the decision trees is set to 4. The test results for different time steps Δt are shown in Table 3.

Table 3

Sample test of the traffic regression model based on the random forest algorithm

Δt	Sample size	Training score	Test score
0.4	1103	0.56	0.68
0.8	370	0.96	0.87
1.2	213	0.99	0.36

Note: *The training score and test score are fitting evaluations between 0 and 1, where 0 is the worst and 1 is the best.*

From the above table and Fig. 16, a time step of Δt = 0.8 seconds is selected as the average time interval for predicting flow, leading to the final grain flow model constructed as [t_0, t_0 + 0.8].

$$Q = f(1.25S_1, 1.25S_2, 1.25S_3,) \quad (4)$$

In the equation, the dynamic output method for flow is as follows: first, the discrete integral area [S_1, S_2, S_3] for each monitoring unit over each second is calculated. Each discrete integral area is divided by the time step Δt to obtain the input array $[x_1, x_2, x_3]$. Subsequently, based on the trained Random Forest flow regression model, the flow values after internal evaluation are output.

Sensor performance test verification

To further validate the monitoring accuracy of the grain flow sensor, a field harvesting verification experiment was conducted in November 2023 at Jiangsu University's experimental field. The selected plot was relatively flat, with the rice variety being Changnong Jing 10, a bulk density of 639 g/L, and a grain moisture content of 21%. The test machine used was a 4LZ-6.0 multifunctional intelligent combine harvester, operating at a feed rate of 6 kg/s and a cutting width of 2.2 m. The experimental site is shown in Fig. 16(a), with the GPS positioning device mounted on the top of the cab, and the grain flow sensor installed as depicted in Fig. 16(b).

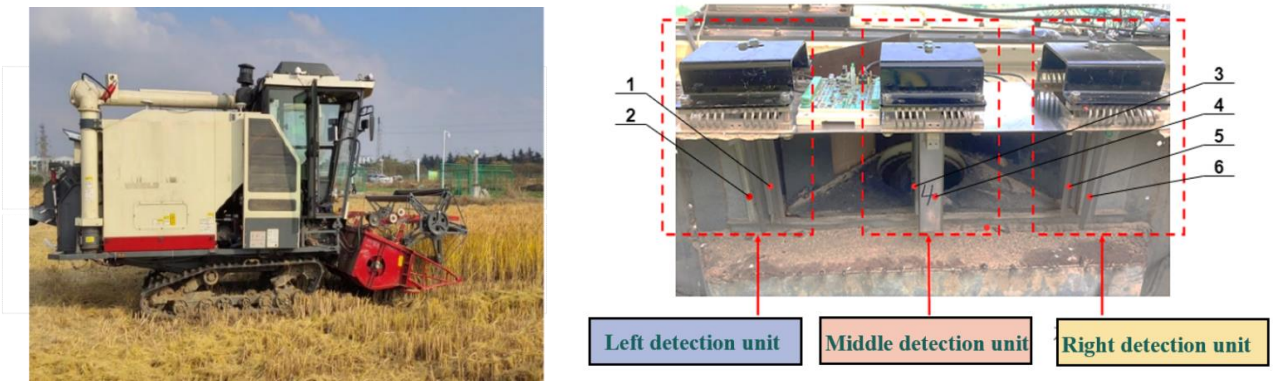

(a) Testing machine (b) Sensor installation diagram

Fig .16 - Physical map of the sensor installation

1. Left impact unit. 2. Left reference unit. 3. Middle impact unit. 4. Middle reference unit. 5. Right impact unit. 6. Right reference unit.

The rice yield measurement validation experiment consisted of five groups, with a uniform harvesting speed over a full cutting width of 30 meters. Cumulative yield data from the grain flow sensor were recorded alongside manual weighing data to compare and verify the sensor's field accuracy. The results are summarized in Table 4. The field trial indicated that the designed grain flow sensor achieved satisfactory monitoring performance, with monitoring errors ranging from -6.42% to 8.23% during stable harvesting conditions.

Table 4

Validation test results

Crop	Actual Quality (kg)	Random Forest Regression Model	
		Predicted Quality (kg)	Error (%)
Rice	122.49	132.57	8.23%
	105.13	99.43	-5.42%
	94.23	97.49	3.46%
	97.28	91.04	-6.42%
	119.39	125.19	4.85%

Discussion

This study addresses the uneven dispersal characteristics of grain ejection from auger outlets by designing an array-type grain flow sensor that utilizes a multi-point distribution and dual-board differential arrangement for monitoring grain flow. However, this study did not consider the impacts of machine tilt and varying grain moisture content. Future work will incorporate tilt sensors to capture the machine's inclination and moisture monitoring sensors to assess grain moisture variations. Additionally, the grain dispersal patterns under different operating conditions will be analyzed and the yield measurement model will be optimized to enhance the versatility of the grain flow sensor developed in this study.

While this research primarily focused on rice crops, the monitoring principles indicate that the developed grain flow sensor is applicable to a variety of crops. Future experimental studies will be conducted on rice, wheat, rapeseed, and other crops to develop a universal grain flow sensor. Furthermore, by integrating positional information from the harvesting machine, it is aimed to generate visualized yield distribution maps to guide precision farming and management for the next crop season.

CONCLUSIONS

To monitor the flow variation of rice grains in real-time, a multi-point monitoring and dual-board differential scheme was proposed based on the dispersal characteristics of grains ejected from the auger outlet of a crawler-type combine harvester, leading to the design of an array-type differential grain flow sensor.

The differential effects of the original signals from the flow sensor were compared in both the frequency and time domains, alongside various filtering and noise reduction methods. The optimal signal processing approach was identified as frequency-domain differentiation combined with "median filtering + first-order filtering," resulting in stable sensor signals.

A grain flow measurement model for rice was constructed using the Random Forest algorithm, and field harvest experiments were conducted for validation. The results indicated that the measurement error during stable field operations ranged from -6.42% to 8.23%.

ACKNOWLEDGEMENT

Shandong Province Key Research and Development Plan (Science and Technology Demonstration Project) Project (2022SFGC0201), Jiangsu Agricultural Science and Technology Independent Innovation Fund Category I project (CX (22) 1005), The Natural Science Foundation of Jiangsu Province (BK20230544), Postgraduate Research & Practice Innovation Program of Jiangsu Province (KYCX22_3678) and Postgraduate Research & Practice Innovation Program of Jiangsu Province (KYCX24_3989).

REFERENCES

1. Bantchina, B.B., Qaswar, M., Arslan, S., Ulusoy, Y., Gündoğdu, K. S., Tekin, Y., Mouazen, A. M. (2024). Corn yield prediction in site-specific management zones using proximal soil sensing, remote sensing, and machine learning approach. *Computers and Electronics in Agriculture, 225,* 109329. https://doi.org/10.1016/j.compag.2024.109329
2. Cheng, S., Han, H., Qi, J., Ma, Q., Liu, J. An, D., Yang, Y. (2023). Design and Experiment of Real-Time Grain Yield Monitoring System for Corn Kernel Harvester. *Agriculture, 13,* 294. https://doi.org/10.3390/agriculture13020294
3. He, Y., Zhou, J., Sun, J., Jia, H., Liang, Z., Awuah. E. (2023). An adaptive control system for path tracking of crawler combine harvester based on paddy ground conditions identification. *Computers and Electronics in Agriculture, 210,* 107948. https://doi.org/10.1016/j.compag.2023.107948

4. Hu, J.W., Luo, X.W., Ruan, H., Chen, S.R., Li, Y.M. (2009). Design of a dual-plate differential impact-based yield sensor (双板差分冲量式谷物流量传感器设计). *Transactions of the Chinese Society for Agricultural Machinery, 40(4)*, 69-72. http://dx.doi.org/10.3969/j.issn.1000-1298.[year].4.[sequence] (China)
5. Li, X.C., Li, M.Z., Zheng, L.H., Zhang, M., Wang, X.J., Sun, M.Z. (2015). Test and optimization of sampling frequency for yield monitor system of grain combine harvester (谷物联合收获机测产系统采样频率优化与试验). Nongye Jixie Xuebao/Trans. *Transactions of the Chinese Society for Agricultural Machinery, 46(S1),* 74-78. http://dx.doi.org/10.6041/j.issn.1000-1298.2015.S0.013 (China)Vinod Chandra, S.S., Anand Hareendran, S., Ghassan, F. A. (2024). Precision farming for sustainability: An agricultural intelligence model. *Computers and Electronics in Agriculture, 226,* 109386. https://doi.org/10.1016/j.compag.2024.109386
6. Liu, R., Zhang, Z., Zhang, M., Yang, W., Li, M. (2018). Performance analysis and modelling of impact-based sensor in yield monitor system. *IFAC-PapersOnLine 51(17),* 613–618. https://doi.org/10.1016/j.ifacol.2018.08.129
7. Kasera, R.K.; Gour, S.; Acharjee, T. (2024). A comprehensive survey on IoT and AI based applications in different pre-harvest, during-harvest and post-harvest activities of smart agriculture. *Computers and Electronics in Agriculture, 216,* 108522. https://doi.org/10.1016/j.compag.2023.108522
8. Ma, Z., Traore, S.N., Zhu, Y., Li, Y., Xu, L., Li, Y. (2022). DEM simulations and experiments investigating grain tank discharge of a rice combine harvester. *Computers and Electronics in Agriculture, 198,* 107060. https://doi.org/10.1016/j.compag.2022.107060
9. Ravishankar, M., Siddharth, S., Yadav, A. A., Kassa, S.R. (2023). Integrating IoT and Sensor Technologies for Smart Agriculture: Optimizing Crop Yield and Resource Management. *2023 IEEE Technology & Engineering Management Conference-Asia Pacific (TEMSCON-ASPAC). IEEE,* 1-5. https://doi.org/10.1109/TEMSCON-ASPAC59527.2023.10531339
10. Shoji, K., Itoh, H., Kawamura, T. (2009). In-situ non-linear calibration of grain-yield sensor: Optimization of parameters for flow rate of grain vs. force on the sensor. *Engineering in Agriculture, Environment and Food, 2(3), 78-82*, https://doi.org/10.1016/S1881-8366(09)80008-6
11. Yin, C., Zhang, Q., Mao, X., Chen, D., Huang, S., Li, Y. (2024). Research of real-time corn yield monitoring system with DNN-based prediction model. *Frontiers in Plant Science*, 15, 1453823. https://doi.org/10.3389/fpls.2024.1453823
12. Wei, X.H., Zhang, J.M., Dan, Z.M., Liu, C.L. (2014). Signal processing method of impact-based grain flow sensor for predicted yield (冲量式谷物流量传感器测产信号处理方法). *Transactions of the Chinese Society of Agricultural Engineering*, *30(15),* 222-228. (China) http://www.tcsae.org/article/doi/10.3969/j.issn.1002-6819.2014.15.029
13. Xing, S., Yu, Y., Cao, G., Hu, J., Zhu, L., Liu, J., Wu, Q., Li Q., Xu L. (2024). Design and Parametric Optimization Study of an Eccentric Parallelogram-Type Uprighting Device for Ratoon Rice Stubbles. *Agriculture, 14(4)*, 534. https://doi.org/10.3390/agriculture14040534
14. Zhao, J., Zhao, H., Tang, H., Wang, X., Yu, Y. (2023). Bionic threshing component optimized based on MBD-DEM coupling simulation significantly improves corn kernel harvesting rate. *Computers and Electronics in Agriculture, 212, 108075.* https://doi.org/10.1016/j.compag.2023.108075
15. Zhou, X., Xu, X., Zhang, J., Wang, L., Wang, D., Zhang, P. (2023). Fault diagnosis of silage harvester based on a modified random forest. *Information Processing in Agriculture, 10(3),* 301-311. https://doi.org/10.1016/j.inpa.2022.02.005